Research Square

Preprints are preliminary reports that have not undergone peer review.
They should not be considered conclusive, used to inform clinical practice,
or referenced by the media as validated information.

Chitosan-Guided Directed In Situ Formation of Zinc- and/or Manganese-Based Phosphate Nanostructures

Benjamín Valdez-Salas
Instituto de Ingeniería, Universidad Autónoma de Baja California
Karen Guillén-Carvajal
kguillen@uabc.edu.mx

Instituto de Ingeniería, Universidad Autónoma de Baja California
Jorge Salvador-Carlos
Instituto de Ingeniería, Universidad Autónoma de Baja California
Ernesto Beltrán-Partida
Instituto de Ingeniería, Universidad Autónoma de Baja California
Jimena Chairez-Gonzalez
Instituto de Ingeniería, Universidad Autónoma de Baja California
Jhonathan Castillo-Saenz
Instituto de Ingeniería, Universidad Autónoma de Baja California
Roberto Gamboa-Becerra
Instituto de Ingeniería, Universidad Autónoma de Baja California

Research Article

Keywords: In situ synthesis, molecular docking, bioactive nanostructure, micro-nanoparticles

Posted Date: March 25th, 2026

DOI: https://doi.org/10.21203/rs.3.rs-9054221/v1

License: This work is licensed under a Creative Commons Attribution 4.0 International License. Read Full License

Additional Declarations: No competing interests reported.

Abstract

In the present work, metal phosphate nanostructures were synthesized *in situ* using a natural polymer-assisted route based on chitosan (CS) and employing zinc and/or manganese as metal precursors. CS acted as a multifunctional matrix capable of regulating the nucleation, growth, and colloidal behavior of the formed nanostructures through electrostatic and coordination interactions with zinc and/or manganese phosphates, also highlighting the decisive role of the type of metal in these processes. The formation mechanism and structural properties of the systems obtained were investigated using FTIR, FE-SEM/EDS, DLS and molecular docking. FTIR analysis confirmed the participation of CS protonated amino groups in acid-base and coordination interactions with metal ions, while characteristic phosphate vibrations evidenced the formation of phosphate phases. Morphological analysis revealed that Mn-containing systems generate hemispherical structures embedded in the polymer matrix, while Zn-containing systems exhibit larger, oblong morphologies with a greater tendency towards aggregation and precipitation. DLS results showed broad size distributions and time-dependent colloidal instability, particularly in zinc-containing systems. Molecular docking simulations provided mechanistic information, showing that phosphate groups have a significantly higher binding affinity for CS compared to isolated metal ions. These results demonstrate that metal-polymer affinity and metal-phosphate coordination rigidity are key parameters in the structural and colloidal control of *in situ* synthesized metal phosphate nanostructures.

Introduction

The synthesis of multifunctional nanocomposites has become one of the main pillars of modern materials science, due to the growing demand for materials with specific properties for biomedical, environmental, and catalytic applications [1]. Although polymer-based materials are still widely used for biomedical applications, they are often subject to rejection and incompatibility with the human body [2]-[7]. Recent advances in green chemistry have focused on the use of biomolecules, which is why biopolymer-based nanocomposites have attracted significant attention due to their biocompatibility, biodegradability, and versatility in adequately hosting inorganic phases [8], [9].

A suitable biomolecule for this purpose is chitosan (CS). CS is a biopolymer derived from the deacetylation of chitin, obtained from insects, fungi and mainly crustaceans [10]-[12]. CS has been widely used for its unique physicochemical properties including: cationic charge, film-forming ability, affinity for metal ions and wide range of application (cosmetology, pharmaceuticals, medical devices, agriculture, etc.), due to its biocompatibility, biodegradability, and bioactivity [13]-[18]. In the field of bone tissue regeneration, CS promotes cell growth and adhesion, has osteoinductive properties and promotes new bone formation [16], [19]-[23]. In addition, CS also has antimicrobial and

immunomodulatory activity, imparting hemostasis [13], [24], [25]. In fact, CS has been used as a coating for inorganic NPs, as well as a drug delivery system [26]-[30].

On the other hand, ascorbic acid (AA), in addition to acting as a pH regulator and providing the characteristic properties of vitamin C, has also been used as a reducing agent and stabilizer in the synthesis of nanoparticles (NPs) [31]-[34]. AA not only modulates the kinetics of the reaction, but also provides antioxidant properties, which are essential for stabilizing metal ions prone to oxidation, such as Mn^{+2} [9].

Transition metal phosphates have been extensively researched due to their superior redox properties with promising applications in heterogeneous catalysis [35]. In the specific case of manganese phosphate NPs, $Mn_3(PO_4)_2$ (MnP in the biological field, they have been used in the efficient and selective transport of drugs [36], as well as detectors and controllers of superoxide anions released by living cells [37]. Like MnP, zinc phosphate NPs, $Zn_3(PO_4)_2$ (ZnP), have been studied for the transport of various compounds to biomimic and generate therapeutic effects [38]-[40]. However, in the biomedical field, specifically in bones, they have not been studied in depth [41]-[43]. Conventional synthesis methods for these materials often involve adverse conditions, such as high temperatures or toxic reagents, which limits their compatibility with biopolymers and environmentally friendly processing. Furthermore, the aggregation of inorganic phases within polymer matrices remains a persistent challenge, requiring innovative strategies to improve dispersion and interfacial interactions [44], [45].

The integration of CS/AA solutions with transition metal phosphates offers a promising avenue for the development of hybrid materials with synergistic functionalities, such as antimicrobial activity, controlled ion release, and promotion of osteoinduction [46], [47]. The use of transition metal complexes as active components, such as zinc and manganese phosphates for the functionalization of polymeric materials, could represent a novel strategy for the production of materials for use in bone rehabilitation that has not been previously investigated [35], [48].

In this context, this work focuses on the *in situ* synthesis of CS and $Zn_3(PO_4)_2$ (CS-ZnP) and/or $Mn_3(PO_4)_2$ (CS-MnP; and/or CS-Zn/MnP) nanostructures, and their respective characterization, with a focus on understanding the role of CS in their formation and stabilization.

Methods and Materials

Materials

Zinc chloride ($ZnCl_2$), manganese chloride tetrahydrate ($MnCl_2•4H_2O$), and monopotassium phosphate (KH_2PO_4) were purchased from FAGALab, Mexico. Ascorbic acid (AA) was obtained from Fisher, Mexico, while low molecular weight chitosan (CS) was obtained from Sigma Aldrich, USA. Distilled water was obtained from Hwater, Mexico.

Synthesis of Nanoparticled Systems

5 mL of a CS/AA solution at a 1:0.7 weight ratio was left in an ultrasonic bath (Branson S800, frequency of 22 kHz at 40% amplitude, 200 W) for 5 min, and 5 mL of a 0.05 M KH_2PO_4 solution was added. The mixture was left to mix for 10 min and then 5 mL of a $MnCl_2•4H_2O$ (0.025 M) solution or a $ZnCl_2$ (0.05 M) solution, or a 1:1 mixture of these, was added drop by drop, depending on the type of particle to be synthesized, under continuous stirring for another 10 min. Finally, the mixture obtained was subjected to ultrasonication for 10 min in an ultrasonic homogenizer (OMNI SONIC RUPTOR 400) at 22 kHz and 40% amplitude, using an acoustic control chamber. The solutions were stored in amber containers at 4°C and in the absence of light. To collect the micro (MCPs) and nanoparticles (NPs), the solution was left to dry in a desiccator for 48 h, after which the solid was collected and ground. The procedure is illustrated in **Fig. 1.**

Physicochemical and morphological characterization of nanoparticles

The functional groups present in the NPs synthesized using a polymer solution were identified by Fourier transform infrared spectroscopy (FTIR) using a PerkinElmer Frontier spectrometer. The spectra were acquired in the wavenumber range from 4000 to 500 cm^{-1} with a resolution of 1 cm^{-1} [49].

The morphology, particle size, and elemental composition were analyzed using Field Emission Scanning Electron Microscopy (FE-SEM; LYRA 3 Tescan) operating at an acceleration voltage of 10 kV and using a secondary electron detector. Prior to analysis, the samples were individually dispersed in absolute ethanol, deposited on double-sided carbon tape, and allowed to dry at room temperature. Elemental chemical analysis was performed using energy dispersive X-ray spectroscopy (EDS, Bruker, Xflash 6I30) coupled to FE-SEM, operating at 10 kV. To optimize the count rate during spectrum acquisition, a large spot size was used [49].

The hydrodynamic size distribution and colloidal stability of the nanoparticles were evaluated by dynamic light scattering (DLS, Microtrac MRB Nanotrac Wave II) in a range of 2 to 500 nm, at room temperature and with a run time of 30 seconds. Additionally, the

diameter distribution was determined by analyzing images obtained by microscopy, using ImageJ 1.54 software (National Institutes of Health) [50].

Molecular Docking

Ligand preparation

The ligands used for the molecular docking study were developed based on previous work by Valdez-Salas et al. [51]. The 3D structures of Mn^{+2}, Zn^{+2} and PO_4^{-3} ions were downloaded from PubChem in SDF format. The molecule was optimized using the Avogadro program, selecting the automatic optimization tool, the MMFF94s force field, four steps per update, and the gradient descent algorithm. The optimized structure was saved in mol2 format.

The ligands were prepared in AutoDockTools 1.5.6 software, following the protocol proposed by Rizvi et al. [52]. Briefly, Gasteiger charges were calculated, the root was selected and detected in the torsion tree, and the torsions were defined. Finally, the ligands were saved in pdbqt format.

Receiver preparation

To evaluate the interaction of ions with the polymer template, the strategy of analyzing a chitosan chain was used. The 3D structures of the CS chain were downloaded from PubChem in SDF format. The molecule was optimized using the Avogadro program, selecting the automatic optimization tool, the MMFF94s force field, four steps per update, and the gradient descent algorithm. The optimized structure was saved in PDB format.

The receptor was prepared in AutoDockTools 1.5.6 software following the protocol proposed by Rizvi et al. [52]. Briefly, Kollman charges representing the charge distribution of complex molecules and hydrogens were added, water molecules were removed, and the files were saved in pdbqt format.

Interactions and binding energy

The results of the molecular docking were evaluated using AutoDockTools. The selected active site corresponds to the entire chain; therefore, the grid had coordinates 70X, 120Y, 70Z, a spacing of 0.325, and a box center of 0X, 0Y, 0Z. Finally, for docking, the general Lamarckian analysis (4.2) was performed, selecting the interaction with the lowest free energy among 10 docking conformations.

Results

In situ synthesized nanoparticles mediated by natural polymers

The *in situ* synthesis of NPs using natural polymer solutions means that the biopolymer performs multiple functions simultaneously. These include acting as a stabilizing agent by regulating the nucleation and growth processes of the NPs; as a reducing agent or soft template by mediating the interaction between metal ions and the functional groups of the polymer; and as a structural matrix that promotes the homogeneous dispersion of the NPs within the colloidal system prior to induced precipitation.

In this study, NPs were synthesized in a colloidal system in the presence of Mn, and precipitated phases were formed in the presence of Zn. In the first case (CS-MnP), the polymer serves a dual function as a stabilizing agent and as a template, while in the CS-ZnP and CS-Zn/MnP systems, the polymer regulates nucleation and particle growth but does not provide colloidal stabilization (Scheme 1). The precipitation of a white solid during synthesis is a common indicator of ZnP formation [50].

These differences are attributed to the different coordination affinity between metal cations and the CS polymer. Mn has lower hydrolysis energy and moderate affinity for the amino ($-NH_2$) and hydroxyl ($-OH$) groups of CS, allowing partial coordination without complete displacement of the solvent. This weak and dynamic interaction favors the stabilization of metal or phosphate nuclei within the polymer matrix, preventing their aggregation. In contrast, Zn exhibits a higher affinity for the electron-donating groups of CS, leading to stronger coordination and restricting the conformational mobility of the polymer. In addition, there is greater coordination with PO_4^{-3} groups, which induces precipitation. As a result, CS cannot reorganize itself adequately to stabilize the formed nuclei, promoting the precipitation of a defined phase corresponding to CS-ZnP or CS-Zn/MnP systems [53].

FTIR analysis of CS/AA and NPs systems

Figure 2 shows the FTIR spectra corresponding to the systems obtained by CS/AA-assisted synthesis. Both pure CS and the CS/AA system exhibited characteristic bands of chitosan [54]. A broad band centered at 3304 cm^{-1} was observed, attributed to $\nu_1(N-H)$ and $\nu_1(O-H)$, stretching vibrations, as well as signals at 2878 cm^{-1} and 2880 cm^{-1}, corresponding to $C-H$ stretching vibrations of the methylene groups.

In the CS spectrum, the band located around 1650 cm^{-1} is associated with the vibration of the carbonyl group ($C=O$) and the $\delta(NH_2)$ deformation. The bands located at 1418 cm^{-1}, 1376 cm^{-1}, 1320 cm^{-1}, and 1318 cm^{-1} 1 are related to $\delta(C-H)$ flexions and $C-N$ vibrations, while the signals at 1070 cm^{-1} and 1024 cm^{-1} correspond to $C-O$ stretching

[55]. Additionally, the peaks at 1150 cm^{-1} and 892 cm^{-1} are characteristic of the $C-O-C$ glycosidic bond of CS.

For its part, the CS/AA spectrum showed an increase in intensity of the band located at 1574 cm^{-1}, attributed to $C=C$ tensions and the protonation of amino groups (NH_2 a NH_3^+) as a result of the acid-base interaction between CS and AA. The presence of a band at 1714 cm^{-1} confirms the incorporation of carbonyl groups from AA [48], [55].

In contrast, the MCPs and NPs corresponding to the CS-MnP, CS-ZnP, and CS-ZnP/MnP systems exhibited intense bands at 1067 cm^{-1}, 1081 cm^{-1} and 1070 cm^{-1}, respectively, associated with vibrations of phosphate groups and $C-O$ bonds [47]. Likewise, shifts and a significant decrease in intensity were observed in the region between 1510 $cm^{-1}$and 1680 cm^{-1}, corresponding to $C=O$ and NH_2 vibrations. When comparing these spectra with the CS/AA system, these variations suggest the interaction of metal ions with the NH_3^+ groups of CS, giving rise to the formation of coordinated complexes, which explains the attenuation of the bands in this spectral region [56].

On the other hand, the peaks at 3266 cm^{-1}, 3356 cm^{-1} and 3346 cm^{-1} are attributed to $O-H$ and $N-H$ stretching vibrations, while the attenuated signals between 1300 cm^{-1} and 1380 cm^{-1} correspond to $C-H$ and $C-N$ vibrations, which were also present in the CS and CS/AA spectra. In particular, in the CS-MnP system, a shift towards lower wave numbers (red shift) of the $O-H$ and $N-H$ bands was observed, suggesting the formation of new hydrogen bonds within the polymer matrix [57]. In contrast, for the CS-ZnP and CS-Zn/MnP systems, these peak bands showed a shift towards higher wave numbers (blue shift), which can be attributed to the modification of the chemical environment of these groups, possibly associated with the formation of weaker hydrogen bonds induced by coordination with Zn^{+2} [58].

In the particular case of CS-ZnP, the band located at 1759 cm^{-1} is associated with the presence of carboxylate groups ($COO-$) from AA, as well as with the increase in the vibrational frequency of the $C=O$ bond, resulting from the electrostatic attraction between the carbonyl oxygen electrons and the Zn^{+2} cations [59]. Meanwhile, the signal observed at 947 cm^{-1} is attributed to vibrations of the $O-P-O$ and $P-O-Zn$ bonds [39], [40]. Finally, the bands detected at 518 cm^{-1} and 511 cm^{-1} in the CS-MnP and CS-Zn/MnP systems, respectively, correspond to $O-P-O$ bending vibrations, typical of phosphate compounds [38], [39].

Morphological Analysis and Synthesis Mechanism

Figures 3a, b, show the morphology of the structures obtained for each system depending on the base metal used during synthesis. In the case of CS-MnP, hemispherical structures embedded in the polymer matrix were observed, with an average diameter of 228 nm. For the CS-ZnP system, brick-like oblong morphologies were identified, with an average width of 406 nm. Finally, the CS-Zn/MnP biphasic NPs exhibited a denser and more compact polymer matrix, in which hemispherical structures with an average size of 169 nm predominated, showing a marked tendency to precipitate.

According to Wang et al [48], the mechanism of spherical structure formation is governed by the initial interaction between CS and phosphate groups **(**Fig. 3c**).** When CS is dissolved in an acidic medium, the primary amines in its polymeric backbone become protonated, acquiring a positive charge. Under these conditions, the CS chains tend to intertwine due to the decrease in electrostatic repulsions between charged segments [60], [61]. Upon addition of the PO_4^{-3} solution (from KH_2PO_4) the protonated amines of CS interact electrostatically with the phosphate anions [21], [62]. Subsequently, in the presence of the solution containing the metal base, the PO_4^{-3} groups anchored to the CS chains attract Mn^{+2} and/or Zn^{+2} ions, promoting the *in situ* formation of MnP, ZnP, or Zn/MnP on the CS surface.

During this process, the growth of MCPs and NPs is restricted by the aggregation and intertwining of long CS chains, which limits the space available for nucleation and crystal growth [24], [48].

DLS Analysis

Figure 4 shows the results of the DLS analysis for MCPs and NPs. A high dispersion in the hydrodynamic sizes obtained was observed, which is mainly attributed to the presence of CS polymer chains in solutions, whose conformation and entanglement contribute to a wide size distribution.

In the case of the CS-Zn/MnP system, the results show that, although the particles were initially dispersed within the nanometric range (8.32 nm), a progressive aggregation process occurred over the course of approximately one day. This phenomenon led to the formation of larger aggregates (11.42 nm – 87.8% Vol) and, finally, to the precipitation of both MCPs and NPs, which is consistent with the behavior observed macroscopically (1.685 µm – 87.8% Vol).

With regard to the ζ potential values, extreme readings were obtained, which can be explained by the high conductivity of the medium (1.5–1.6 mS cm^{-1}). This high conductivity causes compression of the electric double layer around the particles, interfering with electrophoretic measurement and limiting the quantitative reliability of the ζ potential. Taken together, these results are consistent with an unstable system,

characterized by the formation of aggregates and their subsequent precipitation over time.

EDS Analysis

Figure 5 shows the results of the EDS analysis, which confirm the presence of the characteristic elements of each synthesized system. In the case of CS-MnP, signals corresponding to Mn, P, and O were detected; for CS-ZnP, Zn, P, and O were identified; while in the CS-Zn/MnP system, the coexistence of both metals (Mn and Zn) together with P and O was observed, as well as their distribution based on elemental mapping. The traces of C are attributed to the CS polymer matrix and the AA used during synthesis. Likewise, the Cl and K signals are associated with residues from the precursors used in the synthesis process.

Molecular Docking

Molecular coupling simulations showed relatively low direct bond energies for Mn^{+2} (-0.628 kcal mol^{-1}) and Zn^{+2} (-0.452 kcal mol^{-1}) with the functional groups of CS, indicating weak isolated ion-polymer interactions. These results reflect localized and idealized interactions and do not take into account the effects of hydrolysis, metal speciation, ionic size, or cooperative coordination in aqueous media. In contrast, phosphate exhibited a significantly more favorable interaction energy (-7.040 kcal mol^{-1}), acting as the main anchoring fraction within the polymer matrix. This behavior is clearly illustrated in Fig. 6, where phosphate preferentially binds to regions rich in amino and hydroxyl groups, inducing localized structural reorganization (Fig. 6a). On the other hand, when CS interacts with the metal (Fig. 6b **and c**), both Mn^{+2} and Zn^{+2} are preferentially located near the amino groups.

This hierarchical interaction scheme is fully consistent with the proposed synthesis pathway, in which phosphate-driven nucleation precedes metal incorporation. Therefore, the experimentally observed differences between Mn- and Zn-containing systems are not attributed to stronger direct metal-CS interactions, but rather to the greater structural stability and rigidity of Zn-PO_4^{-3} coordination, which promotes nucleation and precipitation of defined CS-ZnP phases, while the more labile coordination of Mn^{+2} favors dynamic stabilization of nuclei within the CS network.

Conclusions

In this work, we demonstrate that chitosan acts as an effective and multifunctional polymeric matrix for the *in situ* synthesis of metal phosphate micro- and nanoparticles, where the nature of the metal cation plays a decisive role in the nucleation, growth, and colloidal stability of the system. FTIR analyses confirmed the involvement of acid-base and

coordination interactions between the protonated amino groups of CS, phosphate anions, and metal cations, while morphological studies revealed that Mn favors the formation of stabilized hemispherical structures within the polymer matrix, in contrast to systems containing Zn, which exhibit more defined morphologies and a marked tendency toward aggregation and precipitation.

The DLS results showed limited, time-dependent colloidal stability, particularly in systems containing Zn, consistent with the greater structural rigidity of Zn-PO_4^{-3} coordination. EDS elemental analysis confirmed the successful incorporation of Mn and/or Zn together with P and O in the synthesized systems.

Complementarily, molecular docking studies provided mechanistic evidence supporting the proposed experimental model, showing that phosphate anions have a significantly higher affinity for CS than isolated metal cations. These results confirm that nucleation is dominated by CS-PO_4^{-3} interactions, followed by interaction with metals.

The combination of the elements proposed in this work and the modulation of the inherent properties of the material could allow these systems to be explored as functional platforms for the development of bioactive materials to be applied in skin and bone tissue engineering.

Declarations

Acknowledgments

We give thanks to Instituto de Ingeniería of Universidad Autónoma de Baja California, and SECIHTI.

Author Contributions

Conceptualization, B. V.-S., and K. G.-C.; methodology, B. V.-S., and K. G.-C.; investigation, K. G.-C., J. S.-C., and J. C.-G.; software, J. S.-C., and J. C.-S.; resources, B. V.-S., and K. G.-C.; writing—original draft preparation, B. V.-S., K. G.-C., and E. B.-P.; writing—review and editing, E. B.-P., R. G.-B., and J. S.-C.; supervision, B. V.-S., and E. B.-P.; formal analysis, K. G.-C., J. S.-C., J. C.-G., and J. C.-S; visualization, K. G.-C. and R. G.-B.; validation, B. V.-S., K. G.-C., and J. S.-C.; project administration, K. G.-C. All authors have read and agreed to the final version of the manuscript.

Funding

No funds, grants, or other support was received.

Data availability

No datasets were generated or analyzed during the current study.

Conflict of interest

The authors declare no conflict of interest. The authors have no financial or proprietary interest in any material discussed in this article.

Ethics approval and consent to participate

Not applicable.

Consent for publication

All authors have read and agreed to the published version of the manuscript.

Materials availability

Not applicable.

Code availability

Not applicable.

References

1. A. Shavandi, P. Saeedi, M. A. Ali, and E. Jalalvandi, “Green synthesis of polysaccharide-based inorganic nanoparticles and biomedical aspects,” in *Functional Polysaccharides for Biomedical Applications*, Elsevier, 2019, pp. 267–304. doi: 10.1016/B978-0-08-102555-0.00008-X.
2. H. Petite *et al.*, “Tissue-engineered bone regeneration,” *Nat. Biotechnol.*, vol. 18, no. 9, pp. 959–963, Sep. 2000, doi: 10.1038/79449.
3. W. E. Fibbe, F. Dazzi, and K. LeBlanc, “MSCs: science and trials,” *Nat. Med.*, vol. 19, no. 7, pp. 812–813, Jul. 2013, doi: 10.1038/nm.3222.
4. M. Ansari and M. Eshghanmalek, “Biomaterials for repair and regeneration of the cartilage tissue,” *Biodes. Manuf.*, vol. 2, no. 1, pp. 41–49, Mar. 2019, doi: 10.1007/s42242-018-0031-0.
5. M. G. A. Vieira, M. A. da Silva, L. O. dos Santos, and M. M. Beppu, “Natural-based plasticizers and biopolymer films: A review,” *Eur. Polym. J.*, vol. 47, no. 3, pp. 254–263, Mar. 2011, doi: 10.1016/j.eurpolymj.2010.12.011.
6. K. Wasilewska and K. Winnicka, “Ethylcellulose–A Pharmaceutical Excipient with Multidirectional Application in Drug Dosage Forms Development,” *Materials*, vol. 12, no. 20, p. 3386, Oct. 2019, doi: 10.3390/ma12203386.

7. M. Ansari, “Bone tissue regeneration: biology, strategies and interface studies,” *Prog. Biomater.*, vol. 8, no. 4, pp. 223–237, Dec. 2019, doi: 10.1007/s40204-019-00125-z.
8. E. Davidson, J. Pereira, G. Gan Giannelli, Z. Murphy, V. Anagnostopoulos, and S. Santra, “Multi-Functional Chitosan Nanovesicles Loaded with Bioactive Manganese for Potential Wound Healing Applications,” *Molecules*, vol. 28, no. 16, p. 6098, Aug. 2023, doi: 10.3390/molecules28166098.
9. W. Zhang *et al.*, “Effect of biopolymer chitosan on manganese immobilization improvement by microbial-induced carbonate precipitation,” *Ecotoxicol. Environ. Saf.*, vol. 279, p. 116496, Jul. 2024, doi: 10.1016/j.ecoenv.2024.116496.
10. V. G. Muir and J. A. Burdick, “Chemically Modified Biopolymers for the Formation of Biomedical Hydrogels.,” *Chem. Rev.*, vol. 121, no. 18, pp. 10908–10949, Sep. 2021, doi: 10.1021/acs.chemrev.0c00923.
11. D. Elieh-Ali-Komi and M. R. Hamblin, “Chitin and Chitosan: Production and Application of Versatile Biomedical Nanomaterials.,” *Int. J. Adv. Res. (Indore).*, vol. 4, no. 3, pp. 411–427, Mar. 2016.
12. D. Gómez-Ríos, R. Barrera-Zapata, and R. Ríos-Estepa, “Comparison of process technologies for chitosan production from shrimp shell waste: A techno-economic approach using Aspen Plus ®,” *Food and Bioproducts Processing*, vol. 103, pp. 49–57, May 2017, doi: 10.1016/j.fbp.2017.02.010.
13. I. M. Wong-Miramontes *et al.*, “Development and Evaluation of Chitosan Active Films for Food Packaging Materials: A New Exoskeleton Source,” *ChemistrySelect*, vol. 10, no. 14, Apr. 2025, doi: 10.1002/slct.202402708.
14. P. K. Dutta, S. Tripathi, G. K. Mehrotra, and J. Dutta, “Perspectives for chitosan based antimicrobial films in food applications,” *Food Chem.*, vol. 114, no. 4, pp. 1173–1182, Jun. 2009, doi: 10.1016/j.foodchem.2008.11.047.
15. I. Aranaz *et al.*, “Cosmetics and Cosmeceutical Applications of Chitin, Chitosan and Their Derivatives,” *Polymers (Basel).*, vol. 10, no. 2, p. 213, Feb. 2018, doi: 10.3390/polym10020213.
16. K. Guillén-Carvajal, B. Valdez-Salas, E. Beltrán-Partida, J. Salomón-Carlos, and N. Cheng, “Chitosan, Gelatin, and Collagen Hydrogels for Bone Regeneration,” *Polymers (Basel).*, vol. 15, no. 13, p. 2762, Jun. 2023, doi: 10.3390/polym15132762.
17. C. P. Jiménez-Gómez and J. A. Cecilia, “Chitosan: A Natural Biopolymer with a Wide and Varied Range of Applications,” *Molecules*, vol. 25, no. 17, p. 3981, Sep. 2020, doi: 10.3390/molecules25173981.
18. D. Policastro *et al.*, “New Zinc-Based Active Chitosan Films: Physicochemical Characterization, Antioxidant, and Antimicrobial Properties,” *Front. Chem.*, vol. 10, May 2022, doi: 10.3389/fchem.2022.884059.

19. A. Di Martino, M. Sittinger, and M. V. Risbud, “Chitosan: A versatile biopolymer for orthopaedic tissue-engineering,” *Biomaterials*, vol. 26, no. 30, pp. 5983–5990, Oct. 2005, doi: 10.1016/j.biomaterials.2005.03.016.
20. J. Venkatesan and S.-K. Kim, “Chitosan Composites for Bone Tissue Engineering—An Overview,” *Mar. Drugs*, vol. 8, no. 8, pp. 2252–2266, Aug. 2010, doi: 10.3390/md8082252.
21. F. Croisier and C. Jérôme, “Chitosan-based biomaterials for tissue engineering,” *Eur. Polym. J.*, vol. 49, no. 4, pp. 780–792, Apr. 2013, doi: 10.1016/j.eurpolymj.2012.12.009.
22. H. Ehrlich, “Chitin and collagen as universal and alternative templates in biomineralization,” *Int. Geol. Rev.*, vol. 52, no. 7–8, pp. 661–699, May 2010, doi: 10.1080/00206811003679521.
23. E. Do Nascimento *et al.*, “Tailoring Drug Release Properties by Gradual Changes in the Particle Engineering of Polysaccharide Chitosan Based Powders,” *Polymers (Basel).*, vol. 9, no. 7, p. 253, Jun. 2017, doi: 10.3390/polym9070253.
24. B. Choi, D.-H. Jo, A. K. M. M. Anower, S. M. S. Islam, and S. Sohn, “Chitosan as an Immunomodulating Adjuvant on T-Cells and Antigen-Presenting Cells in Herpes Simplex Virus Type 1 Infection,” *Mediators Inflamm.*, vol. 2016, pp. 1–12, 2016, doi: 10.1155/2016/4374375.
25. L. Papadimitriou, M. Kaliva, M. Vamvakaki, and M. Chatzinikolaidou, “Immunomodulatory Potential of Chitosan- *graft* -poly(ε-caprolactone) Copolymers toward the Polarization of Bone-Marrow-Derived Macrophages,” *ACS Biomater. Sci. Eng.*, vol. 3, no. 7, pp. 1341–1349, Jul. 2017, doi: 10.1021/acsbiomaterials.6b00440.
26. S. M. Ahsan, M. Thomas, K. K. Reddy, S. G. Sooraparaju, A. Asthana, and I. Bhatnagar, “Chitosan as biomaterial in drug delivery and tissue engineering,” *Int. J. Biol. Macromol.*, vol. 110, pp. 97–109, Apr. 2018, doi: 10.1016/j.ijbiomac.2017.08.140.
27. V. Mikušová and P. Mikuš, “Advances in Chitosan-Based Nanoparticles for Drug Delivery,” *Int. J. Mol. Sci.*, vol. 22, no. 17, p. 9652, Sep. 2021, doi: 10.3390/ijms22179652.
28. L. A. Frank, G. R. Onzi, A. S. Morawski, A. R. Pohlmann, S. S. Guterres, and R. V. Contri, “Chitosan as a coating material for nanoparticles intended for biomedical applications,” *React. Funct. Polym.*, vol. 147, p. 104459, Feb. 2020, doi: 10.1016/j.reactfunctpolym.2019.104459.
29. M. H. Elkomy, A. A. Ali, and H. M. Eid, “Chitosan on the surface of nanoparticles for enhanced drug delivery: A comprehensive review,” *Journal of Controlled Release*, vol. 351, pp. 923–940, Nov. 2022, doi: 10.1016/j.jconrel.2022.10.005.
30. M. Karayianni, T. Sentoukas, A. Skandalis, N. Pippa, and S. Pispas, “Chitosan-Based Nanoparticles for Nucleic Acid Delivery: Technological Aspects, Applications, and

Future Perspectives," *Pharmaceutics*, vol. 15, no. 7, p. 1849, Jun. 2023, doi: 10.3390/pharmaceutics15071849.

31. M. Iliut, C. Leordean, V. Canpean, C.-M. Teodorescu, and S. Astilean, "A new green, ascorbic acid-assisted method for versatile synthesis of Au–graphene hybrids as efficient surface-enhanced Raman scattering platforms," *J. Mater. Chem. C Mater.*, vol. 1, no. 26, p. 4094, 2013, doi: 10.1039/c3tc30177j.
32. L. Malassis, R. Dreyfus, R. J. Murphy, L. A. Hough, B. Donnio, and C. B. Murray, "One-step green synthesis of gold and silver nanoparticles with ascorbic acid and their versatile surface post-functionalization," *RSC Adv.*, vol. 6, no. 39, pp. 33092–33100, 2016, doi: 10.1039/C6RA00194G.
33. K. Guzmán, B. Kumar, M. Grijalva, A. Debut, and L. Cumbal, "Ascorbic Acid-assisted Green Synthesis of Silver Nanoparticles: pH and Stability Study," in *Green Chemistry - New Perspectives*, IntechOpen, 2022. doi: 10.5772/intechopen.107202.
34. T. J. Jayeoye *et al.*, "Exploration of Biocompatible Ascorbic Acid Reduced and Stabilized Gold Nanoparticles, as Sensitive and Selective Detection Nanoplatform for Silver Ion in Solution," *Plasmonics*, Jul. 2024, doi: 10.1007/s11468-024-02413-2.
35. J. C. Munyemana, H. He, S. Ding, J. Yin, P. Xi, and J. Xiao, "Synthesis of manganese phosphate hybrid nanoflowers by collagen-templated biomineralization," *RSC Adv.*, vol. 8, no. 5, pp. 2708–2713, 2018, doi: 10.1039/C7RA12628J.
36. J. Yu, R. Hao, F. Sheng, L. Xu, G. Li, and Y. Hou, "Hollow manganese phosphate nanoparticles as smart multifunctional probes for cancer cell targeted magnetic resonance imaging and drug delivery," *Nano Res.*, vol. 5, no. 10, pp. 679–694, Oct. 2012, doi: 10.1007/s12274-012-0252-z.
37. M.-Q. Wang, C. Ye, S.-J. Bao, and M.-W. Xu, "Controlled synthesis of Mn3(PO4)2 hollow spheres as biomimetic enzymes for selective detection of superoxide anions released by living cells," *Microchimica Acta*, vol. 184, no. 4, pp. 1177–1184, Apr. 2017, doi: 10.1007/s00604-017-2112-8.
38. A. J. Jadhav *et al.*, "Development of Smart Nanocontainers With A Zinc Phosphate Core and A pH-Responsive Shell for Controlled Release of Immidazole," *Hybrid Materials*, vol. 2, no. 1, Jan. 2015, doi: 10.1515/hyma-2015-0001.
39. A. J. Jadhav, D. V. Pinjari, and A. B. Pandit, "Surfactant assisted sonochemical synthesis of hollow structured zinc phosphate nanoparticles and their application as nanocarrier," *Chemical Engineering Journal*, vol. 297, pp. 116–120, Aug. 2016, doi: 10.1016/j.cej.2016.04.001.
40. K. Kumar and P. Paik, "Biomimicked and CPMV-Imprinted Hollow Porous Zinc Phosphate Nanocapsules and Their Therapeutic Efficiency," *ACS Appl. Bio Mater.*, vol. 3, no. 9, pp. 6005–6014, Sep. 2020, doi: 10.1021/acsabm.0c00634.

41. B. R. Barrioni, E. Norris, S. Li, P. Naruphontjirakul, J. R. Jones, and M. de M. Pereira, “Osteogenic potential of sol–gel bioactive glasses containing manganese,” *J. Mater. Sci. Mater. Med.*, vol. 30, no. 7, p. 86, Jul. 2019, doi: 10.1007/s10856-019-6288-9.
42. F. Westhauser *et al.*, “Effect of manganese, zinc, and copper on the biological and osteogenic properties of mesoporous bioactive glass nanoparticles,” *J. Biomed. Mater. Res. A*, vol. 109, no. 8, pp. 1457–1467, Aug. 2021, doi: 10.1002/jbm.a.37136.
43. Q. Nawaz *et al.*, “Synthesis and characterization of manganese containing mesoporous bioactive glass nanoparticles for biomedical applications,” *J. Mater. Sci. Mater. Med.*, vol. 29, no. 5, p. 64, May 2018, doi: 10.1007/s10856-018-6070-4.
44. R. Y. Hong and Q. Chen, “Dispersion of Inorganic Nanoparticles in Polymer Matrices: Challenges and Solutions,” 2014, pp. 1–38. doi: 10.1007/12_2014_286.
45. A. K. M. M. Alam, “Methods of nanoparticle dispersion in the polymer matrix,” in *Nanoparticle-Based Polymer Composites*, Elsevier, 2022, pp. 469–479. doi: 10.1016/B978-0-12-824272-8.00008-7.
46. A. Soriente *et al.*, “Chitosan/hydroxyapatite nanocomposite scaffolds to modulate osteogenic and inflammatory response,” *J. Biomed. Mater. Res. A*, vol. 110, no. 2, pp. 266–272, Feb. 2022, doi: 10.1002/jbm.a.37283.
47. J. V. Rau *et al.*, “Sic Parvis Magna: Manganese-Substituted Tricalcium Phosphate and Its Biophysical Properties,” *ACS Biomater. Sci. Eng.*, vol. 5, no. 12, pp. 6632–6644, Dec. 2019, doi: 10.1021/acsbiomaterials.9b01528.
48. Y. Wang *et al.*, “Constructing high effective nano-Mn3(PO4)2-chitosan in situ electrochemical detection interface for superoxide anions released from living cell,” *Biosens. Bioelectron.*, vol. 133, pp. 133–140, May 2019, doi: 10.1016/j.bios.2019.03.029.
49. B. Valdez-Salas *et al.*, “Synthesis of $Zn_3(PO_4)_2$ and $Mn_3(PO_4)_2$ nanoparticles from aqueous and ethanolic extracts of *Mentha aquatica* and *Mentha spicata*,” *Green Chem. Lett. Rev.*, vol. 18, no. 1, Dec. 2025, doi: 10.1080/17518253.2025.2539745.
50. B. Valdez-Salas, K. Guillén-Carvajal, E. Beltrán-Partida, J. Salvador-Carlos, M. Curiel-Álvarez, and N. Nedev, “Synthesis of stable suspension zinc-phosphate micro/nanoparticles under acid and alkaline conditions,” *Journal of Nanoparticle Research*, vol. 28, no. 1, p. 4, Jan. 2026, doi: 10.1007/s11051-025-06527-4.
51. B. Valdez-Salas *et al.*, “Nasal Spray Disinfectant for Respiratory Infections Based on Functionalized Silver Nanoparticles: A Physicochemical and Docking Approach,” *Nanomaterials*, vol. 15, no. 7, p. 533, Mar. 2025, doi: 10.3390/nano15070533.
52. S. M. D. Rizvi, S. Shakil, and M. Haneef, “A simple click by click protocol to perform docking: AutoDock 4.2 made easy for non-bioinformaticians.,” *EXCLI J.*, vol. 12, pp. 831–57, 2013.

53. R. B. Hernández, O. R. Yola, and A. L. R. Mercê, “Chemical equilibrium in the complexation of first transition series divalent cations Cu2+, Mn2+ and Zn2+ with chitosan,” *J. Braz. Chem. Soc.*, vol. 18, no. 7, pp. 1388–1396, 2007, doi: 10.1590/S0103-50532007000700015.
54. B. A. Alimi, S. Pathania, J. Wilson, B. Duffy, and J. M. C. Frias, “Extraction, quantification, characterization, and application in food packaging of chitin and chitosan from mushrooms: A review,” *Int. J. Biol. Macromol.*, vol. 237, p. 124195, May 2023, doi: 10.1016/j.ijbiomac.2023.124195.
55. A. B. D. Nandiyanto, R. Oktiani, and R. Ragadhita, “How to Read and Interpret FTIR Spectroscope of Organic Material,” *Indonesian Journal of Science and Technology*, vol. 4, no. 1, p. 97, Mar. 2019, doi: 10.17509/ijost.v4i1.15806.
56. R. B. Hernández *et al.*, “Coordination study of chitosan and Fe3+,” *J. Mol. Struct.*, vol. 877, no. 1–3, pp. 89–99, Apr. 2008, doi: 10.1016/j.molstruc.2007.07.024.
57. Z. Fang, W. Lou, W. Zhang, X. Guan, J. He, and J. Lin, “Modulating crystallinity and dielectric constant of chitosan film for triboelectric polarity shift and performance enhancement in triboelectric nanogenerators,” *Nano Energy*, vol. 117, p. 108923, Dec. 2023, doi: 10.1016/j.nanoen.2023.108923.
58. S. Li *et al.*, “Uncovering the Dominant Role of an Extended Asymmetric Four-Coordinated Water Network in the Hydrogen Evolution Reaction,” *J. Am. Chem. Soc.*, vol. 145, no. 49, pp. 26711–26719, Dec. 2023, doi: 10.1021/jacs.3c08333.
59. J. He, L. Wang, K. Zheng, S. Hu, X. Zhang, and Z. Mu, “Coordination of Mg2+ with Chitosan for Enhanced Triboelectric Performance,” *Polymers (Basel).*, vol. 17, no. 8, p. 1001, Apr. 2025, doi: 10.3390/polym17081001.
60. M. Rinaudo, “Chitin and chitosan: Properties and applications,” *Prog. Polym. Sci.*, vol. 31, no. 7, pp. 603–632, Jul. 2006, doi: 10.1016/j.progpolymsci.2006.06.001.
61. T. Kiang, J. Wen, H. W. Lim, and K. W. Leong, “The effect of the degree of chitosan deacetylation on the efficiency of gene transfection,” *Biomaterials*, vol. 25, no. 22, pp. 5293–5301, Oct. 2004, doi: 10.1016/j.biomaterials.2003.12.036.
62. S. Mao, W. Sun, and T. Kissel, “Chitosan-based formulations for delivery of DNA and siRNA,” *Adv. Drug Deliv. Rev.*, vol. 62, no. 1, pp. 12–27, Jan. 2010, doi: 10.1016/j.addr.2009.08.004.

Scheme 1

Scheme 1 is available in the Supplementary Files section.

Figures

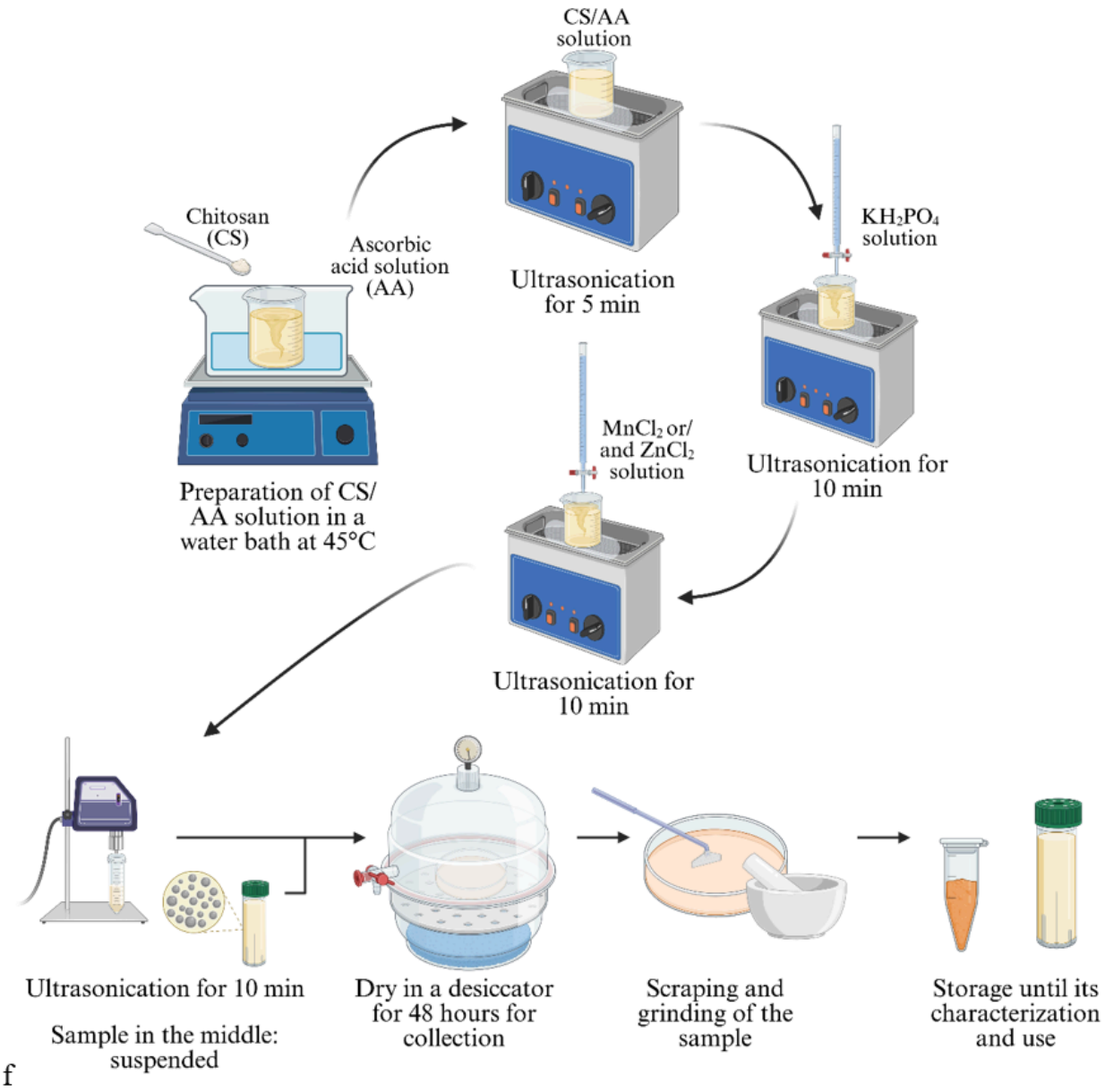


Figure 1

Synthesis method for CS-ZnP, CS-MnP and CS-Zn/MnP. Created in Biorender.

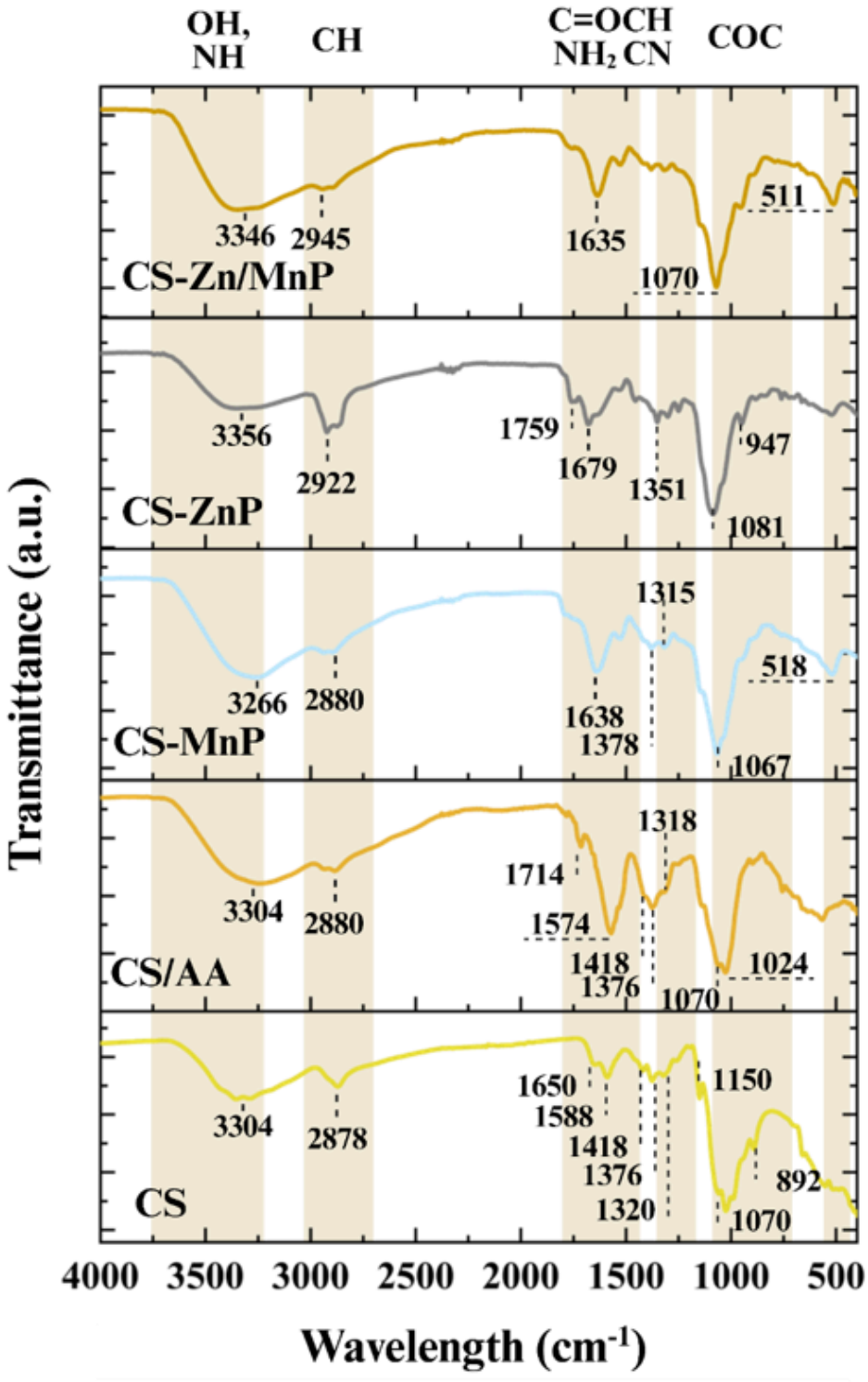


Figure 2

FTIR spectra of CS, CS/AA, and the MCPs and NPs obtained from MnP, ZnP, and Zn/MnP.

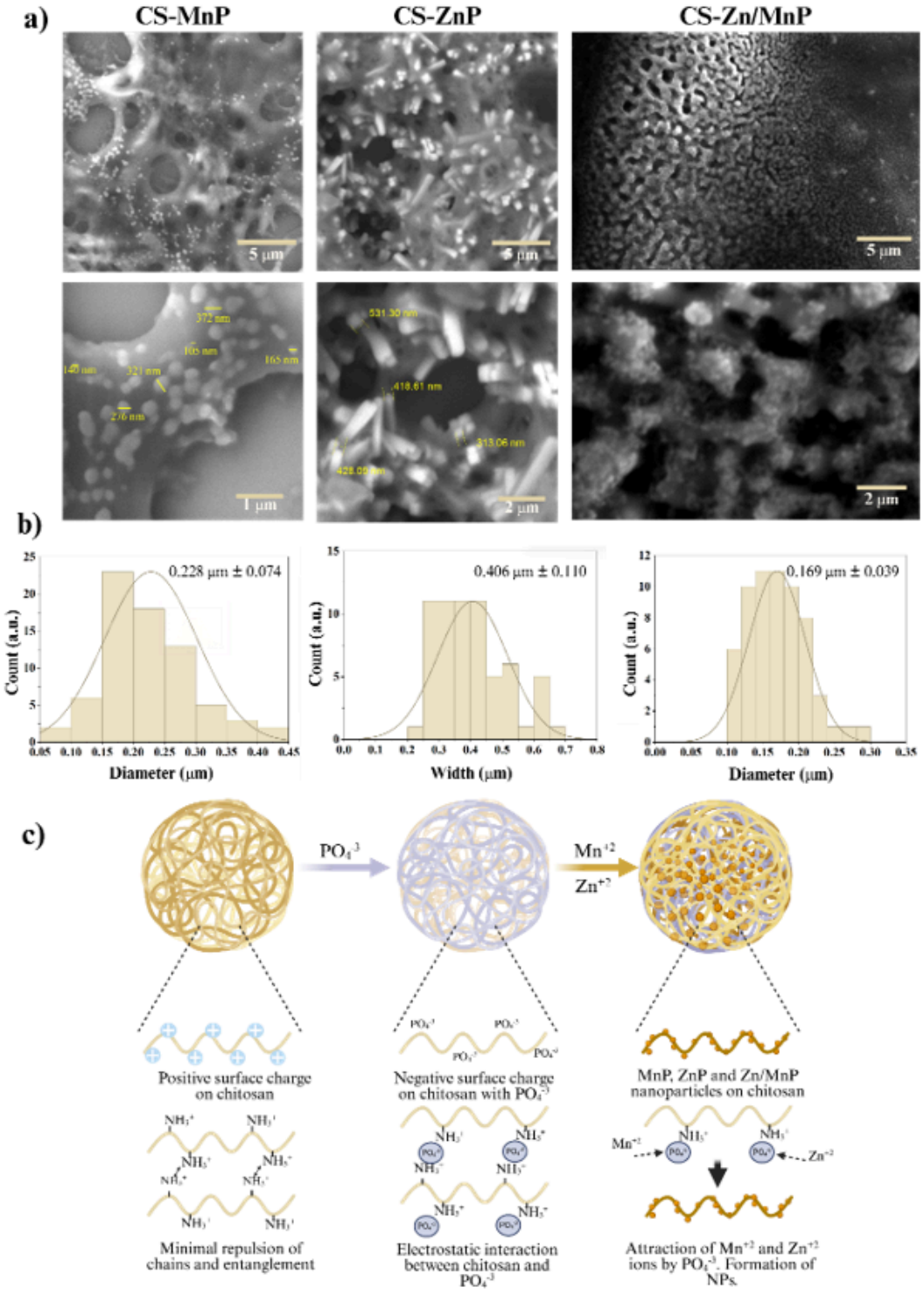


Figure 3

Morphological characterization of NPs synthesized in CS/AA polymeric medium. a) SEM micrographs, b) Size distribution based on SEM micrographs, and c) Formation mechanism (created in Biorender).

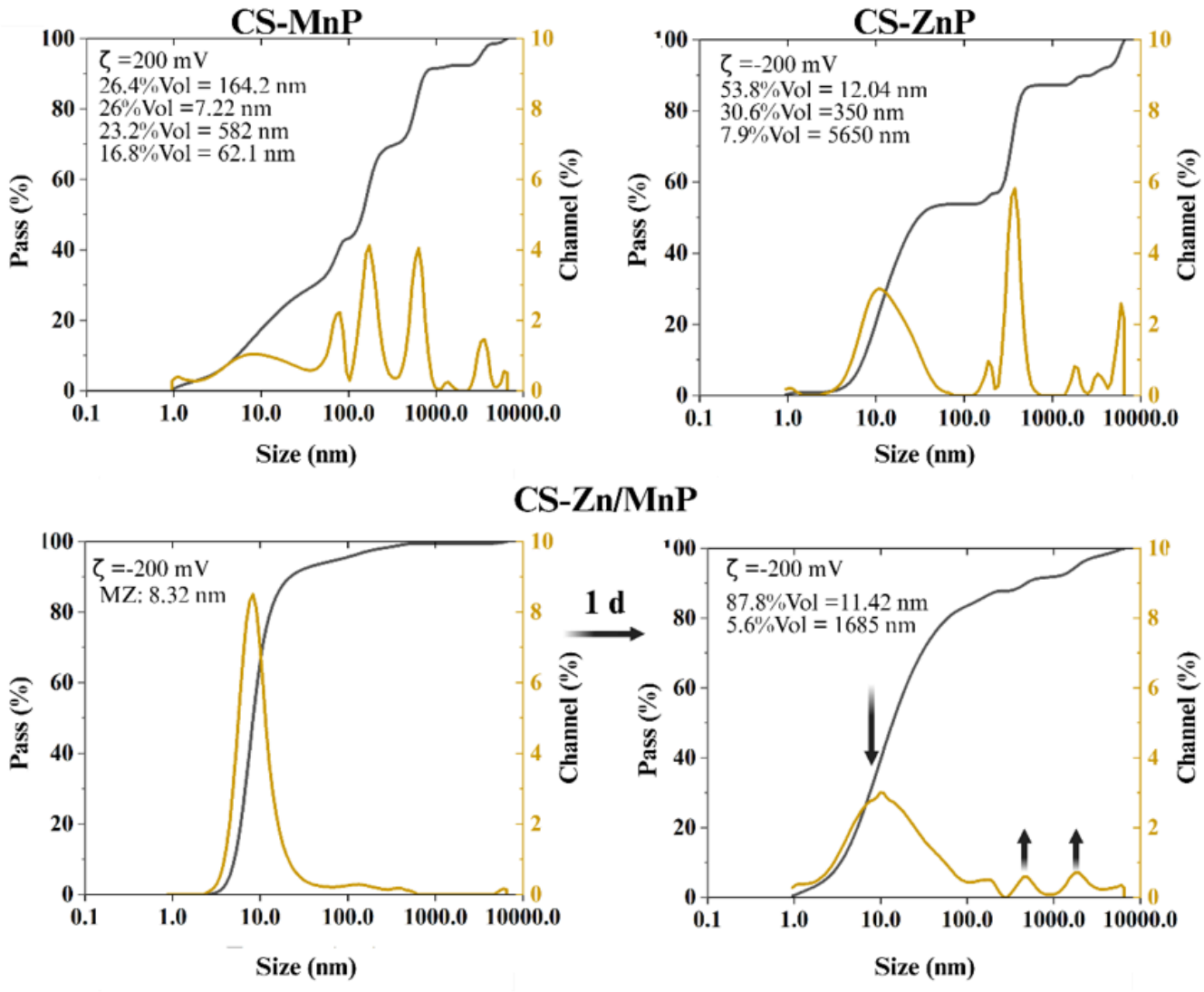
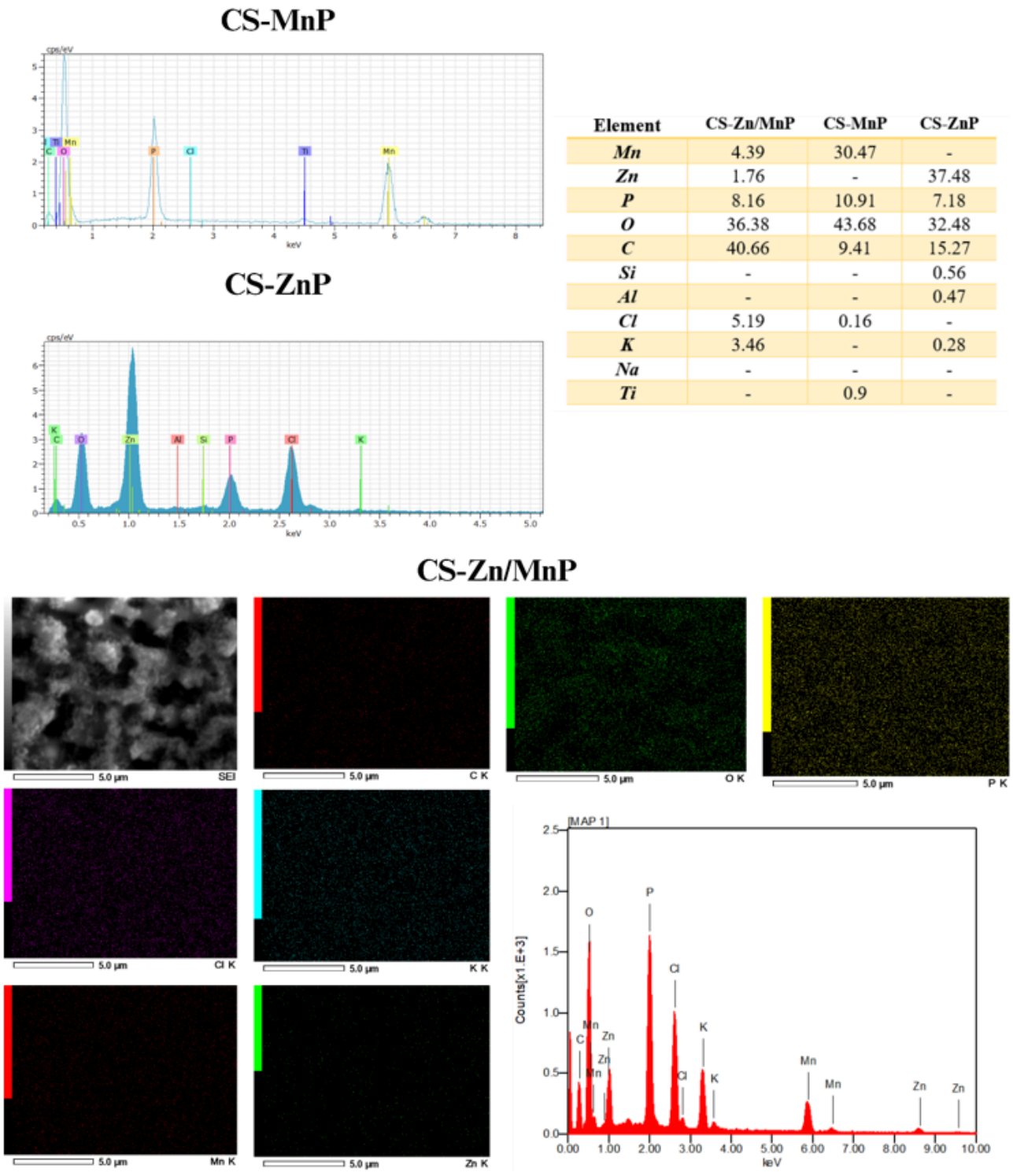


Figure 4

Resultados DLS de CS-MnP, CS-ZnP y CS-Zn/MnP.



Element	CS-Zn/MnP	CS-MnP	CS-ZnP
Mn	4.39	30.47	-
Zn	1.76	-	37.48
P	8.16	10.91	7.18
O	36.38	43.68	32.48
C	40.66	9.41	15.27
Si	-	-	0.56
Al	-	-	0.47
Cl	5.19	0.16	-
K	3.46	-	0.28
Na	-	-	-
Ti	-	0.9	-

Figure 5

EDS analysis of MCPs and NPs synthesized in CS/AA medium and elemental mapping of CS-Zn/MnP.

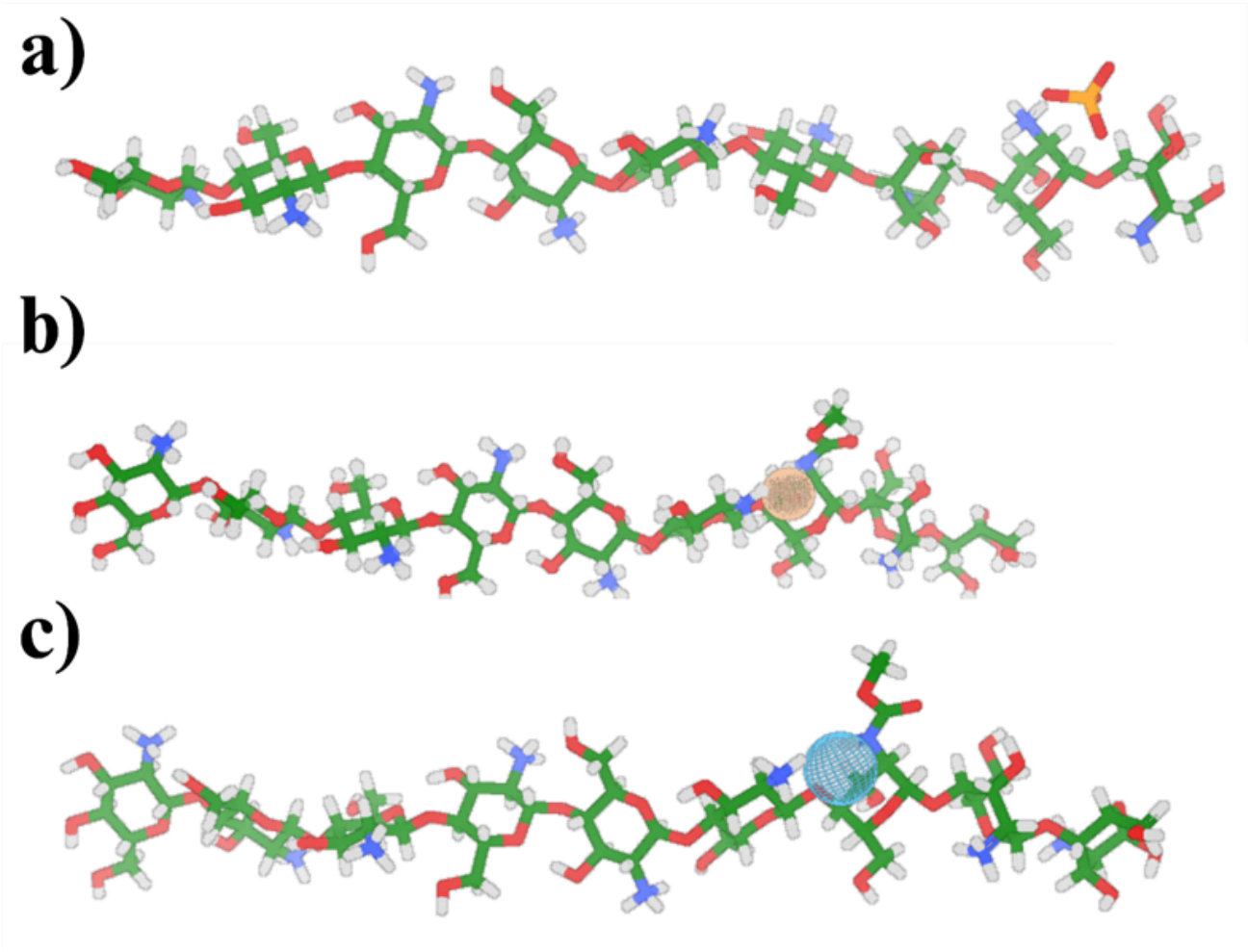


Figure 6

Molecular docking between: a) CS and phosphate; b) CS and Mn^{+2}; and c) CS and Zn^{+2}.

Supplementary Files

This is a list of supplementary files associated with this preprint. Click to download.

- GraphicalAbstract.docx
- Scheme1.docx